AgriEngineering

MDPI

Article

Predictive Modeling of Climate-Driven Crop Yield Variability Using DSSAT Towards Sustainable Agriculture

Safa E. El-Mahroug [1,*], Ayman A. Suleiman [1], Mutaz M. Zoubi [2,*], Saif Al-Omari [3,4], Qusay Y. Abu-Afifeh [1,4], Heba F. Al-Jawaldeh [1,4], Yazan A. Alta'any [4], Tariq M. F. Al-Nawaiseh [4], Nisreen Obeidat [1,4], Shahed H. Alsoud [1,4], Areen M. Alshoshan [1], Fayha M. Al-Shibli [1] and Rakad Ta'any [5]

[1] Department of Land, Water and Environment, The University of Jordan, Amman 11942, Jordan; aymansuleiman510@gmail.com (A.A.S.); qusayyabuafifeh@outlook.com (Q.Y.A.-A.); jaloudiheba@gmail.com (H.F.A.-J.); nisreen.obeidat@yahoo.com (N.O.); shahedsoud95@gmail.com (S.H.A.); areenalshoshan@yahoo.com (A.M.A.); f.shibli@ju.edu.jo (F.M.A.-S.)
[2] Department of Chemistry, The University of Jordan, Amman 11942, Jordan
[3] Department of Water and Environmental Engineering, Scientific Sustainable Vision Company, Amman 11194, Jordan; saifomari116@gmail.com
[4] Department of Civil Engineering, The University of Jordan, Amman 11942, Jordan; yazan.taani@hotmail.com (Y.A.A.); tareq.nawaiseh@gmail.com (T.M.F.A.-N.)
[5] Department of Water Resources and Environmental Management, Al-Balqa' Applied University, Al-Salt 19117, Jordan; rakad.ayed@yahoo.com
* Correspondence: emad.safaa15@yahoo.com (S.E.E.-M.); mutazalzoubi@outlook.com (M.M.Z.)

Abstract: Climate change poses a significant threat to agricultural productivity, particularly in regions vulnerable to extreme temperatures and water scarcity, such as Irbid, Jordan. This study assesses the future impacts of projected shifts in precipitation and temperature on wheat yields, using the Decision Support System for Agrotechnology Transfer (DSSAT) model for calibrating and validating under local agro-environmental conditions. Two shared socioeconomic pathways (SSP3-7.0 and SSP5-8.5), representing high-emission and fossil-fuel-intensive futures, were evaluated across mid- and late-century periods (2030–2060 and 2070–2100). The DSSAT model was calibrated using local field data to simulate crop phenology, biomass accumulation, and nitrogen dynamics, showing strong agreement with observed grain yield and harvest index, thereby confirming its reliability for climate impact assessments. Yield projections under each scenario were further analyzed using machine learning algorithms—random forest and gradient boosting regression—to quantify the influence of individual climate variables. The results showed that under SSP5-8.5 (2030–2060), precipitation was the dominant factor influencing yield variability, underscoring the critical role of water availability. In contrast, under SSP3-7.0 (2070–2100), rising maximum temperatures became the primary constraint, highlighting the growing risk of heat stress. Predictive accuracy was higher in precipitation-dominated scenarios (R^2 = 0.81) than in temperature-dominated cases (R^2 = 0.65–0.73), reflecting greater complexity under extreme warming. These findings emphasize the value of integrating well-calibrated crop models with climate projections and machine learning tools to support climate-resilient agricultural planning. Moreover, practical adaptation strategies, such as adjusting planting dates, using heat-tolerant varieties, and optimizing irrigation, are recommended to enhance resilience. Emerging techniques such as seed priming show promise and merit integration into future crop models. The findings support SDG 2 and SDG 13 by informing climate-resilient food production strategies.

Keywords: climate scenarios; crop–climate interaction; data-driven agriculture; gradient boosting; heat and water stress; machine learning; random forest

check for updates

Academic Editor: Mohammad Valipour

Received: 14 April 2025
Revised: 4 May 2025
Accepted: 13 May 2025
Published: 16 May 2025

Citation: El-Mahroug, S.E.; Suleiman, A.A.; Zoubi, M.M.; Al-Omari, S.; Abu-Afifeh, Q.Y.; Al-Jawaldeh, H.F.; Alta'any, Y.A.; Al-Nawaiseh, T.M.F.; Obeidat, N.; Alsoud, S.H.; et al. Predictive Modeling of Climate-Driven Crop Yield Variability Using DSSAT Towards Sustainable Agriculture. *AgriEngineering* **2025**, *7*, 156. https://doi.org/10.3390/agriengineering7050156

Copyright: © 2025 by the authors. Licensee MDPI, Basel, Switzerland. This article is an open access article distributed under the terms and conditions of the Creative Commons Attribution (CC BY) license (https://creativecommons.org/licenses/by/4.0/).

1. Introduction

Climate change is one of the most pressing global challenges, with far-reaching effects across environmental and socioeconomic sectors [1–3]. Agriculture remains among the most vulnerable, as it is directly affected by climatic factors such as temperature, precipitation, and atmospheric CO_2 concentrations. Wheat, a globally significant staple crop, is particularly sensitive to these fluctuations. Shifts in rainfall distribution and rising temperatures pose substantial threats to its productivity [4,5]. In Jordan, these risks are already evident, with increasing temperatures and decreasing precipitation undermining the performance of rainfed agricultural systems [6]. In this context, the development and evaluation of effective adaptation strategies are imperative. Crop simulation models—particularly the Decision Support System for Agrotechnology Transfer (DSSAT)—offer valuable frameworks for assessing crop performance under projected climate scenarios and testing potential adaptation interventions [7].

Previous studies have employed DSSAT extensively to assess climate impacts on wheat yields and to propose adaptation strategies. Al-Bakri et al. [8] investigated rainfed wheat production in Jordan, highlighting the critical influence of rainfall reduction on yield. Similarly, Waffa and Benoit [9] applied DSSAT in Algeria, exploring adaptation strategies such as adjusting sowing dates and selecting suitable genotypes to cope with changing climate conditions. In Egypt, Dawoud et al. [10] studied the calibration of DSSAT for wheat under various irrigation treatments, recommending optimized irrigation practices to improve crop performance. Jia et al. [11] highlighted accelerated wheat growth yet increased water stress in China's Haihe Basin. In Jordan, studies focusing on Karak and Irbid revealed the significant direct impacts of reduced rainfall on wheat productivity [12–14]. Anbar and Masoud [15] assessed the broader impacts of climate change on agriculture in Egypt, advocating for climate-smart agricultural techniques. Mohamed et al. [16] delved into the economic ramifications of climate change on wheat production in Egypt, underscoring the financial vulnerabilities posed by changing climate conditions. Moreover, Halawa [17] used the AquaCrop model in Syria to simulate maize production under climate change scenarios, focusing on the role of supplemental irrigation, which could also be relevant for wheat production in Jordan. Al-Zraiqat [18] examined the role of agriculture in the broader context of climate change in Jordan, linking land use and water resource management to environmental sustainability. While many of these studies utilize DSSAT or similar crop models to evaluate climate change impacts on wheat, the current research takes a more integrated approach. Unlike previous studies, this research uniquely considers the specific soil and climatic conditions in Jordan, refining adaptation strategies tailored to the local environment. The significance of this research lies in its potential to address Jordan's food security challenges in the face of climate change. Given that Jordan is highly dependent on wheat imports, and its rainfed agricultural system is particularly vulnerable to changing climatic patterns, identifying effective adaptation strategies is crucial for the country's agricultural sustainability [19].

The aim of this study is evaluating wheat production yield under both current and projected climate conditions in Jordan, with a focus on assessing the potential of the Decision Support System for Agrotechnology Transfer (DSSAT) as a decision-making tool for agricultural policy and climate adaptation. The research addresses a critical challenge: the high sensitivity of Jordan's wheat production to climate variability. With declining rainfall and rising temperatures, the sustainability of wheat cultivation in the country faces serious risks. Existing research has not sufficiently explored Jordan-specific adaptation strategies that account for local soil characteristics, nitrogen use efficiency, and climate-resilient wheat genotypes. To bridge this gap, the study involves the application of DSSAT to simulate wheat yield under various climate scenarios. By integrating global modeling

techniques with the localized agricultural context of Jordan, this research contributes valuable insights toward the development of tailored, sustainable production strategies. The study was conducted in Maru village, located in the Irbid Governorate of Jordan, and spans both historical (1990–2020) and projected future periods (2030–2060 and 2070–2100).

2. Materials and Methods

The methodology employed in this study involved the collection of soil and weather data, along with the compilation of experimental records from the Maru Agricultural Research Station, a key wheat cultivation site in Jordan [8]. These datasets were used to calibrate a crop simulation model to estimate wheat yield. For this purpose, the free version of DSSAT 4.6 software was utilized. Historical wheat yield data were sourced from previous research conducted in both farmers' fields and experimental plots at the research station [10]. Information on crop management practices, soil properties, and daily recorded climate data was used to derive and calibrate genotype coefficients specific to the wheat variety under study [20].

Initially, the model was applied to simulate wheat yields for the historical baseline period of 1990–2020. Future yield projections were then generated using climate data from the Max Planck Institute for Meteorology Earth System Model (MPI-ESM1-2-HR), since it has run the experiment of all forcing simulations of the recent past [21,22], under two Shared Socioeconomic Pathway (SSP) scenarios [23]:

- SSP3-7.0: A high-emission scenario characterized by regional rivalry and significant climate impacts.
- SSP5-8.5: A fossil fuel intensive development pathway with very high emissions and extreme warming.

The raw climate data were obtained from the Earth System Grid Federation (ESGF), a widely recognized global repository for climate model datasets [24]. The downscaled data, at a spatial resolution of 25 km, were bias-corrected using the Quantile Mapping Method (QMM) to improve reliability [25]. The subsequent sections provide further detail on the study site, data sources, and specific methodological steps undertaken in this research.

2.1. Study Site Description

The study site was selected to represent a typical rainfed agricultural area in Jordan where wheat is widely cultivated. As shown in Figure 1, the site is located in Irbid Governorate, the country's major producer of wheat and barley, with an annual average production of 6460 tonnes of wheat and 3339 tonnes of barley [8]. This location was chosen due to the availability of comprehensive agricultural data from the Jordan National Agricultural Research Center (NARC) and the Ministry of Agriculture (MoA). The site lies in northern Jordan, within Irbid Governorate (32.64° North, 35.57° East) [24], where data were collected from the Maru and Ramtha agricultural research stations, as well as from farmers' fields. The area is situated at an elevation of approximately 570 m (m) above sea level. It benefits from reliable climatic records, which were obtained from the Ministry of Water and Irrigation (MWI) and National Oceanic and Atmospheric Administration (NOAA). The agricultural research stations operated by NARC support the cultivation of various rainfed crops for research purposes. This region represents a semi-arid Mediterranean environment with varied rainfall and temperature patterns. During the baseline period of 1990–2020, the mean annual rainfall in Irbid was approximately 460 mm (mm). Within the governorate, annual rainfall ranged from 206 mm in the east to 460 mm in the west. Rainfall typically begins in October and ends in May, with the majority occurring between December and March—coinciding with lower air temperatures. Consequently, crop production in this area heavily relies on stored soil moisture. At the Irbid meteorological station, annual

precipitation ranged from a minimum of 214 mm in 1999 to a maximum of 878 mm in 1992. The study area is characterized by mixed land-use activities, including rainfed and irrigated agriculture, open rangeland grazing, and urban development. Rainfed farming in the area includes the cultivation of wheat, barley, olives, and other crops. These crops are grown on diverse soil types, predominantly Typic Xerochrepts, including deep cracking clay soils (Vertisols) found in the Irbid plateau [8].

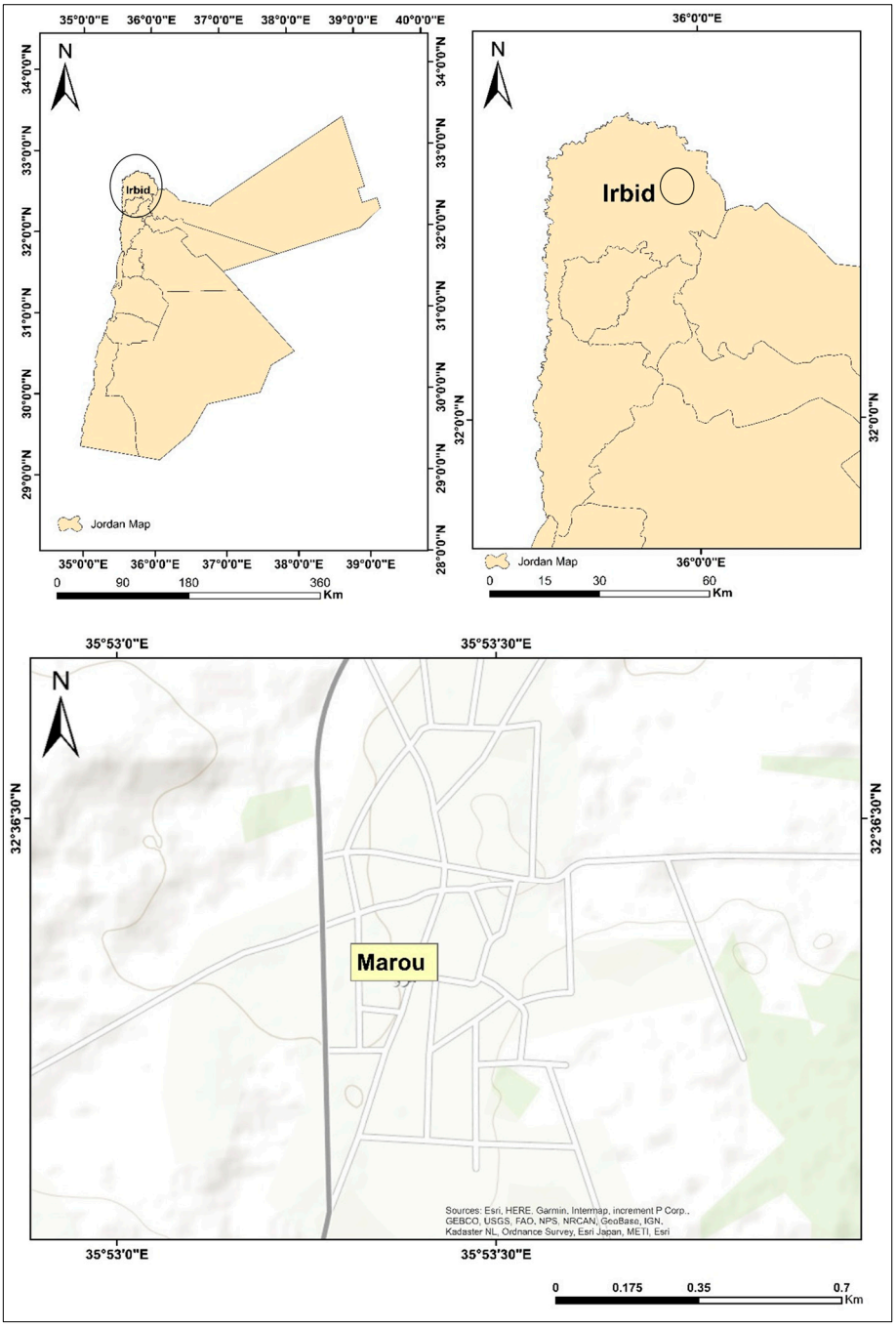


Figure 1. Geographical location of the study area in Maru, Irbid, Jordan.

2.2. Model Selection Justification

The DSSAT was selected for this study due to its well-established performance in simulating crop growth under diverse agro-environmental conditions, particularly in semi-arid and Mediterranean-type climates similar to those of northern Jordan [7,10]. DSSAT's CERES-Wheat module has been extensively validated in comparable environments and is

well suited to simulate key phenological stages, water and nutrient dynamics, and yield responses to varying climatic inputs [20,26].

Compared to other models (Table 1), such as Agricultural Production Systems sIMulator (APSIM) and Simulateur mulTIdisciplinaire pour les Cultures Standard (STICS), DSSAT offers several advantages in the context of this study. APSIM is known for its robust modular design and strong water-use efficiency modeling, particularly for systems with diverse rotations and complex agronomic interactions [27,28]. However, APSIM's calibration often requires extensive site-specific soil and management data, which are not always available or standardized in the Jordanian context. STICS, widely used in European studies, is powerful for managing detailed plant–soil–atmosphere interactions, but its accessibility is limited by language support and region-specific calibration requirements [29,30].

Table 1. Comparative assessment of three widely used crop simulation models (DSSAT, APSIM, and STICS) based on their applicability, strengths, and limitations in simulating crop responses under climate change scenarios.

Criteria	DSSAT [7,10,20]	APSIM [27,28]	STICS [29,30]
Validated in arid/semi-arid regions	Yes	Partially *	No
Supports climate impact analysis (e.g., CMIP/SSP integration)	Yes	Yes	Limited
Requires extensive site-specific calibration	Moderate	Yes	Yes
Suitable for crop rotation and complex farming systems	Limited	Yes	No
Strong in water/nutrient balance simulation	Yes	Yes	Yes
Detailed phenology and yield simulation	Yes	Yes	Yes
Documentation and user support availability	Extensive	Moderate	Limited
Region-specific calibration available for the Middle East	Yes	Limited	No
Used in recent studies in the Mediterranean/Levant region	Yes	Limited	No
Language and accessibility barriers	No	No	Yes **
Open access or freely available	Yes	Yes	Yes

* Partially: it has been used in some Mediterranean contexts but lacks extensive validation or widespread adoption in the region. ** French interface only.

In contrast, DSSAT integrates smoothly with available global datasets (e.g., weather, soil, and management), has strong documentation and support, and is frequently used in conjunction with CMIP-based climate projections. Furthermore, its established application in Middle Eastern studies enhances its credibility for regional comparison. Therefore, DSSAT was deemed the most appropriate model for simulating wheat production in the study area.

2.3. Data Collection and DSSAT Calibration for Wheat Yield Simulation

To calibrate the DSSAT model, comprehensive datasets were obtained from the Maru site in northern Jordan, where the improved wheat variety Acsad-65 is widely cultivated. Site-specific soil characterization data, including texture, bulk density, organic matter content, and hydraulic properties, were provided by the NARC. These locally observed parameters were used to populate the soil profile inputs in DSSAT, enhancing the model's ability to simulate soil water dynamics and nutrient movement under local agro-climatic conditions. Using field-based data instead of default or global soil databases (e.g., SoilGrids) allowed for more representative modeling of the semi-arid environment [31].

Stakeholder perspectives were indirectly incorporated through farmer survey data provided also by the NARC. These surveys, conducted over several years in the Maru region, included information on local agronomic practices, cultivar preferences, planting schedules, and fertilization regimes. The research team had access only to the aggregated results and summary reports, while the original survey instruments and raw data were not made available due to confidentiality restrictions. Although direct stakeholder engagement was not conducted as part of this study, the integration of locally validated farmer practices helped ensure realistic calibration and context-specific interpretation of the modeling results.

DSSAT is recognized for its balance of accuracy and relatively low data requirements, relying on a core set of inputs including daily maximum and minimum temperatures, solar radiation, precipitation, crop management practices, soil characteristics, and crop-specific parameters [20,32].

2.3.1. Soil Profile Input for DSSAT Calibration

In this study, model calibration was tailored to local conditions using field data from the Maru agricultural station and observations from surrounding farms. Essential crop management inputs, such as planting dates (mid to late December) and harvest dates (late April to mid-May), were incorporated. Weather inputs consisted of daily temperature, solar radiation, and rainfall records. Soil data—critical for accurate simulation—included parameters such as upper and lower drainage limits, soil texture, macronutrient content (nitrogen, phosphorus, potassium), pH levels, and other profile-specific properties [8–10,18]. These data, sourced from NARC databases and prior studies [8–10,18], are shown in Table 2.

Table 2. Soil profile input data for DSSAT calibration obtained from NARC.

Soil Depth cm	LL cm^3/cm^3	UL cm^3/cm^3	SAT cm^3/cm^3	ESW cm^3/cm^3	ISW cm^3/cm^3	RDIST cm	ρ_B g/cm^3	pH	OC %
0–5	0.228	0.41	0.48	0.182	0.228	1	1.29	7.5	15
5–15	0.228	0.41	0.48	0.182	0.228	1	1.29	7.5	15
15–30	0.193	0.39	0.47	0.197	0.193	0.64	1.31	7.6	10
30–45	0.2	0.35	0.45	0.15	0.2	0.41	1.37	7.8	10
45–60	0.2	0.35	0.45	0.15	0.2	0.41	1.37	7.8	10
60–90	0.174	0.38	0.46	0.206	0.174	0.22	1.36	7.9	10
90–120	0.2	0.379	0.54	0.179	0.2	0.12	1.38	7.9	10
120–150	0.21	0.37	0.45	0.16	0.21	0.07	1.4	7.9	10

Soils in the study area are generally deep with surface textures of clay loam and silty clay loam, as well as subsurface layers of clay and clay loam. These textures support high water-holding capacity, favoring rainfed agriculture. The soil profile used in the DSSAT model was defined through eight layers extending to a depth of 150 cm. Each layer was characterized by key hydraulic and chemical properties. The lower limit (LL) ranged from 0.174 to 0.228 cm^3/cm^3, while the upper limit (UL) varied between 0.35 and 0.41 cm^3/cm^3. Saturated water content (SAT) spanned from 0.45 to 0.54 cm^3/cm^3. Extractable soil water (ESW) was calculated for each horizon, with values ranging from 0.15 to 0.206 cm^3/cm^3. Initial soil water content (ISW) was set equal to the lower limit for each layer to simulate conservative moisture conditions. Root distribution (RDIST) decreased with depth, from 1.0 cm at the surface to 0.07 cm in the deepest layer (120–150 cm). Bulk density (ρ_B) values ranged between 1.29 and 1.4 g/cm^3, and soil pH was slightly alkaline (7.5–7.9). Organic carbon (OC) content was highest in the surface layers (15%) and decreased to 10% below 15 cm. Chemically, the soils are calcareous with high carbonate content and an average pH of 8.1 [26]. Nutrient levels—particularly nitrogen, phosphorus, and organic matter—were

relatively low, underscoring the need for proper fertilization to optimize yields [33,34]. These inputs were used to represent the local soil conditions for accurate simulation of water and nutrient dynamics in the wheat crop model.

2.3.2. Genetic Coefficients for Wheat Cultivar Calibration

The DSSAT-CERES-Wheat model was calibrated using a set of cultivar-specific genetic coefficients to simulate the phenological development and yield performance of wheat under local agro-climatic conditions. The applied coefficients are shown in Table 3 [35–37].

Table 3. Genotype coefficients for Acsad-65 after calibration and optimization in DSSAT mode.

Coefficient	Value
P1V	5
P1D	90.75
P5	567
G1	22
G2	60
G3	0.5
Phint	119

The P1V coefficient represents the thermal time from seedling emergence to the end of the juvenile phase, during which the plant remains insensitive to photoperiod. P1D refers to the photoperiod sensitivity factor, which quantifies the delay in development (in days) for each hour by which the day length falls below the critical threshold; a value of 70 indicates moderate sensitivity. P5 defines the thermal time (in degree days) from the beginning of grain filling to physiological maturity, with a value of 320 reflecting a relatively extended grain-filling period, which allows for enhanced yield accumulation under favorable conditions.

The yield components are captured through coefficients G1, G2, and G3. Specifically, G1 is a kernel number coefficient that controls potential grain number per unit of stem weight at anthesis. G2 represents the standard kernel weight (in milligrams per kernel) under optimal conditions, while G3 is a tillering coefficient that adjusts the cultivar's potential to produce tillers relative to a reference genotype.

Finally, PHINT is the phyllochron interval, defined as the thermal time (in degree days) between the appearance of successive leaf tips. A value of 119 indicates a moderate leaf development rate and governs canopy expansion. These coefficients were iteratively tuned using observed phenological and yield data to ensure accurate model calibration for the target wheat variety grown in Irbid, Jordan.

The optimization process involved iterative simulations to minimize the root mean square error (*RMSE*) between observed and simulated values. Additionally, the normalized root mean square error (*NRMSE*) was calculated to assess model performance [35,36]. This calibration step was essential to ensure reliable model outputs under both historical and projected climate scenarios. The *RMSE* was computed as shown in Equation (1) [35]:

$$RMSE = \sqrt{\frac{1}{N}\sum_{i=1}^{N}(P_i - O_i)^2} \quad (1)$$

where P_i is the predicted value obtained from DSSAT, N is the number of samples, and O_i is the observed value obtained from farmers' data. Equation (2) for the NRMSE, which represented the degree of variation as [35]

$$NRMSE = \frac{RMSE}{\overline{y}} \times 100 \quad (2)$$

where $\overline{y}$ is the mean value of the predicted and of observed value. The *NRMSE* is similar to the coefficient of variation.

2.4. Statistical and Machine Learning Analysis

Simulations were carried out for the period 1990–2020 using climatic data (wheat production yield (WPY) (kilogram per hectare, kg/ha), mean annual precipitation (MAP) (mm), mean annual radiation (MAR) (kilowatt-hours per square meter, kWh/m^2), mean annual maximum temp (MAXT) (degrees Celsius, °C), and mean annual minimum temp (MANT) (°C)). For the periods 2030–2060 and 2070–2100, ESGF data for SSP3-7.0 and SSP5-8.5 were used. The simulation for 1990–2020 served as the baseline for comparing changes in wheat yield, as shown in Figure 2.

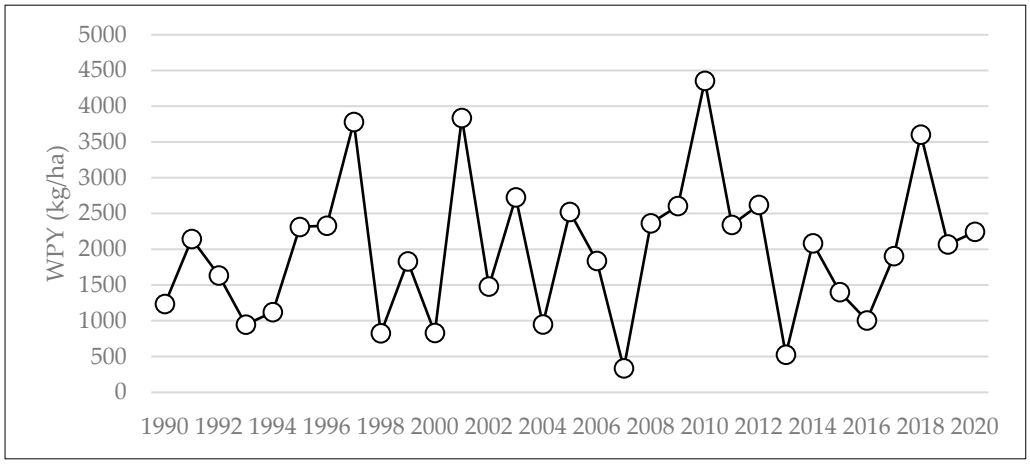


Figure 2. Historical wheat production yield in Maru, Irbid, Jordan, as obtained from NARC.

To evaluate the influence of climatic variables on wheat yield and to develop predictive models, a suite of statistical and machine learning techniques was applied using the R programming language [36,38]. The following steps were undertaken:

- Correlation analysis was conducted to examine the strength and direction of linear relationships between simulated yield and individual climate parameters.
- To evaluate whether the data met the assumptions required for parametric statistical analyses, the Shapiro–Wilk test was employed to assess the normality of the distribution for key continuous variables, including wheat yield, precipitation, maximum and minimum temperature, and solar radiation. This test is widely regarded as one of the most powerful methods for detecting departures from normality, particularly for small to moderate sample sizes. The Shapiro–Wilk test statistic WWW is defined as [35]

$$W = \frac{\left(\sum_{i=1}^{n} a_i x_i\right)^2}{\sum_{i=1}^{n} (x_i - \overline{x})^2} \quad (3)$$

where x_i are the ordered sample values; $\overline{x}$ is the sample mean; and a_i are constants derived from the means, variances, and covariances of the order statistics of a normally

distributed sample. A non-significant result ($p > 0.05$) indicates that the data do not deviate significantly from a normal distribution.

- Two different machine learning algorithms producing decision trees were elaborated to stabilize and improve the prediction modeling process:
- Feature importance analysis was conducted using a random forest model to quantify the relative contribution of each climate variable to yield variability [12]. This model generates multiple decision trees using a bagging technique for supervised prediction purposes regarding the variable sets. For $l = 1\ to\ L$, the main equation is [39]

$$f_{rf}^{L}(x) = \frac{1}{L}\sum_{l=1}^{L} T_b(x) \quad (4)$$

where the random forest tree T_b makes the new point x after selecting the variable randomly, splitting the node of best random variable and then classifying the prediction of l^{th}. This technique improves bagging by using more randomization.

- Predictive modeling was trained on each dataset to derive a predictive equation for wheat yield. We employed the eXtreme Gradient Boosting (XGBoost) algorithm [40], a high-performance ensemble ML technique. The model was trained on the climate-yield dataset to derive predictive equations estimating wheat yield under future scenarios. The algorithm function $f(\theta)$ uses the following main equation to avoid overfitting [41]:

$$f(\theta) = \sum_{i=1}^{N} l(\hat{u}_i,\ u_i) + \sum \Omega(f_k) \quad (5)$$

where $l(\hat{u}_i, u_i)$ and $\Omega(f_k)$ denote the loss error and regularization term, respectively, for the model of tree (f_k) regarding the predicted value $\hat{u}_i$ compared to the actual value u_i of sample for all trees number k^{th}.

Model performance was evaluated using the coefficient of determination (R^2), which measures the proportion of yield variance explained by the model's input variables. Higher R^2 values indicate better predictive accuracy and model fit.

All data analysis and machine learning tasks were implemented using RStudio (version 2024.08.0, Build 463; © 2009–2025 Posit Software, Public Benefit Corporation), utilizing open-source packages for reproducibility and transparency.

To assess model robustness and generalizability, both the random forest and XGBoost models were validated using 10-fold cross-validation, a standard resampling technique that partitions the dataset into ten equal subsets. In each iteration, the model was trained on nine folds and tested on the remaining fold, ensuring that every observation was used for validation once. The random forest model achieved R^2 values of 0.69 and 0.78 under SSP3-7.0 and SSP5-8.5, respectively, while the XGBoost model attained higher predictive accuracy, with R^2 values of 0.75 (SSP3-7.0) and 0.89 (SSP5-8.5). These results confirm that both models reliably captured the underlying relationships between climate variables and yield, with XGBoost offering slightly superior performance across scenarios.

3. Results and Discussion

3.1. Simulation and Validation of Crop–Soil Dynamics and Yield Performance

3.1.1. Crop and Soil Dynamics During Development

The calibrated DSSAT-CERES-Wheat model effectively simulated both the physiological development and biochemical status of the wheat crop across its major phenological stages (Table 4). During early development—sowing, germination, and emergence—no dry matter accumulation or nitrogen uptake was simulated, consistent with the biological dormancy and minimal metabolic activity that characterize the early heterotrophic phase.

Table 4. Simulated crop and soil status at the main development stages in the DSSAT model.

DAP	Growth Stage	Biomass kg/ha	Leaf		Crop Nitrogen		Stress Factor	
			LAI * (m^2/m^2)	Number	kg/ha	%	Water	Nitrogen
0	Sowing	0	0	0	0	0	0	0
5	Germinate	0	0	0	0	0	0	0
10	Emergence	0	0	0	0	0	0	0
70	Terminal Spikelet	1069	0.58	6.8	11	1	0	0
90	End of Vegetative Stage	3393	2.08	9.4	33	1	0	0
102	End of Ear Growth	5794	1.88	9.4	30	0.5	0	0
114	Beginning of Grain Filling	8499	1.68	9.4	52	0.6	0.03	0.01
116	Harvest	8642	1.59	9.4	57	0.7	0	0

* LAI: Leaf Area Index.

By the terminal spikelet stage, the model recorded a biomass accumulation of 1069 kg/ha, alongside a leaf area index (LAI) of 0.58 m^2/m^2, reflecting the establishment of initial photosynthetic surfaces. The crop had developed 6.8 leaves per plant, and nitrogen uptake reached 11 kg/ha, with a nitrogen concentration of 1% in plant tissues, indicating adequate nitrogen assimilation and incorporation into structural and enzymatic proteins.

At the end of the vegetative phase, biomass increased sharply to 3393 kg/ha, accompanied by a peak LAI of 2.08, and maximum leaf number of 9.4, reflecting enhanced canopy photosynthetic capacity. Total crop nitrogen content increased to 33 kg/ha, with nitrogen likely partitioned into chlorophyll, amino acids, and proteins required for leaf expansion and metabolic activity. During the end of ear growth, biomass rose to 5794 kg/ha, although a slight decline in LAI to 1.88 m^2/m^2 suggested the onset of leaf senescence, likely driven by hormonal signaling and nutrient remobilization. At the onset of grain filling, biomass reached 8499 kg/ha, and nitrogen uptake rose to 52 kg/ha, indicating active remobilization from vegetative to reproductive tissues. The tissue nitrogen concentration declined to 0.6%, in line with the dilution effect due to increasing biomass and the shift in allocation toward carbohydrate-rich grain tissues.

Abiotic stress indicators, namely, water stress (H_2O stress) and nitrogen stress (N stress), remained close to zero throughout most stages, except for minor values of 0.03 and 0.01, respectively, at the start of grain filling. This suggests that both osmotic balance and nutrient availability were well maintained, minimizing metabolic disruptions. At harvest, the model simulated a final biomass of 8642 kg/ha and total nitrogen uptake of 57 kg/ha, with LAI further declining to 1.59, reflecting advanced senescence and remobilization of biochemical reserves.

3.1.2. Comparing Simulated and Observed Phenological Stages

The final calibration outputs of the DSSAT-CERES-Wheat model were evaluated against observed data for major physiological and biochemical traits influencing crop productivity (Table 5). Simulated phenological stages were directly compared to field observations in order to examine their potential role in explaining discrepancies in grain yield components. The model accurately predicted early vegetative development, simulating emergence at 10 days after planting (DAP) and anthesis at 105 DAP, both reasonably close to the observed values of 7 and 110 DAP, respectively. However, physiological maturity was not captured correctly, which may be attributed to inaccuracies in thermal time accumulation or photoperiod sensitivity beyond anthesis. This phenological misalignment likely influenced the duration and efficiency of post-anthesis grain filling.

Table 5. Main growth and development variables in the DSSAT model and the measured data obtained from NARC, Jordan.

Variable	Description	Simulated	Measured
Emergence (DAP)	Number of days between sowing and the appearance of the seedling above ground	10	7
Anthesis (DAP)	Number of days from sowing until flowering begins	105	110
Maturity (DAP)	Number of days from sowing until grain development is complete	−99	136
Product wt (kg dm/ha)	Final economic yield (e.g., grain) dry matter per hectare, with no post-harvest losses included	2601	2460
Product unit weight (g dm)	Dry weight of a single grain/unit, in grams; important for yield component analysis	0.018	0.062
Product number (no/m^2)	Number of final products (e.g., grains) per square meter	14,689	4000
Product harvest index (ratio)	Ratio of economic yield (e.g., grain) to total above-ground biomass; HI = Product wt/Biomass; indicates resource allocation efficiency	0.3	0.25
Canopy (tops) wt (kg dm/ha)	Dry weight of above-ground plant parts	8642	9699
Vegetative wt (kg dm/ha)	Dry weight of leaves and stems only	6041	7239

In terms of carbon assimilation and partitioning, the model simulated a grain yield of 2601 kg dry matter (DM)/ha, closely matching the observed value of 2460 kg DM/ha. However, the simulated grain unit mass (0.018 g) was significantly lower than the observed 0.062 g, while the grain number per square meter was overestimated (14,689 vs. 4000), further reinforcing those inaccuracies in reproductive development timing may have contributed to errors in partitioning photosynthates into grain components. Despite this, the harvest index (HI)—the ratio of economic yield to total above-ground biomass—was reasonably estimated at 0.30, compared to the observed 0.25, indicating relatively balanced dry matter allocation under modeled conditions.

The canopy (top biomass) and vegetative biomass were slightly underestimated (8642 and 6041 kg/ha) compared to field observations (9699 and 7239 kg/ha), suggesting a modest underrepresentation of carbon fixation or partitioning to structural tissues. Nitrogen dynamics were captured with higher fidelity. Simulated total nitrogen uptake was 71.2 kg/ha, with 39.1 kg/ha allocated to the grain, leading to a nitrogen harvest index of 0.69. This reflects effective nitrogen remobilization from vegetative tissues to the grain during the reproductive phase. The final grain nitrogen concentration was 1.5%, while vegetative tissues had a concentration of 0.3%, which are consistent with typical values for wheat grown under sufficient nitrogen availability.

Pre-anthesis biochemical data further support this balance: at anthesis, the simulated leaf and stem biomass was 6481 kg/ha, with 30 kg/ha of nitrogen stored in those tissues, and a leaf nitrogen concentration of 3%—a value indicating high metabolic activity and photosynthetic efficiency during flowering. Together, these findings confirm that although minor discrepancies in phenological timing existed, their effects on grain component formation were recognized and interpreted within the calibration framework. Collectively, the model's outputs support its robustness for simulating wheat response to environmental and management variables in nitrogen-sensitive agroecosystems.

In terms of carbon assimilation and partitioning, the model simulated a grain yield of 2601 kg dry matter (DM)/ha, closely matching the observed value of 2460 kg DM/ha. However, the simulated grain unit mass (0.018 g) was significantly lower than the observed 0.062 g, while the grain number per square meter was overestimated (14,689 vs. 4000), indicating a mismatch in the conversion of photosynthates into reproductive organs.

Despite this, the harvest index (HI)—the ratio of economic yield to total above-ground biomass—was reasonably estimated at 0.30, compared to the observed 0.25, indicating relatively balanced dry matter allocation under modeled conditions.

The canopy (top biomass) and vegetative biomass were slightly underestimated (8642 and 6041 kg/ha) compared to field observations (9699 and 7239 kg/ha), suggesting a modest underrepresentation of carbon fixation or partitioning to structural tissues. Nitrogen dynamics were captured with higher fidelity. Simulated total nitrogen uptake was 71.2 kg/ha, with 39.1 kg/ha allocated to the grain, leading to a nitrogen harvest index of 0.69. This reflects effective nitrogen remobilization from vegetative tissues to the grain during the reproductive phase. The final grain nitrogen concentration was 1.5%, while vegetative tissues had a concentration of 0.3%, which are consistent with typical values for wheat grown under sufficient nitrogen availability.

Pre-anthesis biochemical data further support this balance: at anthesis, the simulated leaf and stem biomass was 6481 kg/ha, with 30 kg/ha of nitrogen stored in those tissues, and a leaf nitrogen concentration of 3%—a value indicating high metabolic activity and photosynthetic efficiency during flowering. These findings affirm that the model effectively simulated both the mass flow and biochemical allocation of nitrogen, even if some discrepancies in phenological duration and reproductive partitioning remain. Collectively, the model's outputs support its robustness for simulating wheat response to environmental and management variables in nitrogen-sensitive agroecosystems.

3.2. Crop Yield Under Climate Scenarios Analysis

3.2.1. Descriptive Statistics and Normality Test

The descriptive statistics under the SSP3-7.0 and SSP5-8.5 climate scenarios, shown in Table 6, provide critical insights into the expected variability and distribution of key agro-climatic variables affecting agricultural productivity, especially production yield, precipitation, radiation, and temperature. The projected ten-year averages for the climatic parameters under the SSP3-7.0 and SSP5-8.5 climate scenarios are represented in Figure 3.

Table 6. Summary of the descriptive statistics and normality test.

SSPs	Statistical Parameter	WPY (kg/ha)	MAP (mm)	MAR (kWh/m^2)	MAXT (°C)	MANT (°C)
SSP3-7.0	Mean ± STDV	1119 ± 412	0.49 ± 0.19	18.9 ± 0.09	25.1 ± 1.19	13.2 ± 1.62
	CV	0.37	0.38	0.00	0.05	0.12
	Skewness	0.05	0.70	−0.23	0.13	0.37
	Minimum	151	0.19	18.7	22.8	10.5
	Maximum	2062	1.05	19.1	27.6	16.9
	W	0.98731	0.95938	0.97048	0.98358	0.98118
	p-value	0.77190	0.30858	0.14060	0.57480	0.45790
SSP5-8.5	Mean ± STDV	1048 ± 446	0.49 ± 0.19	18.9 ± 0.08	25.9 ± 1.42	14.0 ± 2.28
	CV	0.43	0.39	0.00	0.05	0.16
	Skewness	−0.51	0.57	0.04	0.03	0.24
	Minimum	0	0.16	18.8	23.3	10.5
	Maximum	1820	1.08	19.1	28.9	19.0
	W	0.96642	0.97547	0.95060	0.98608	0.97502
	p-value	0.08751	0.24890	0.10426	0.70720	0.23660

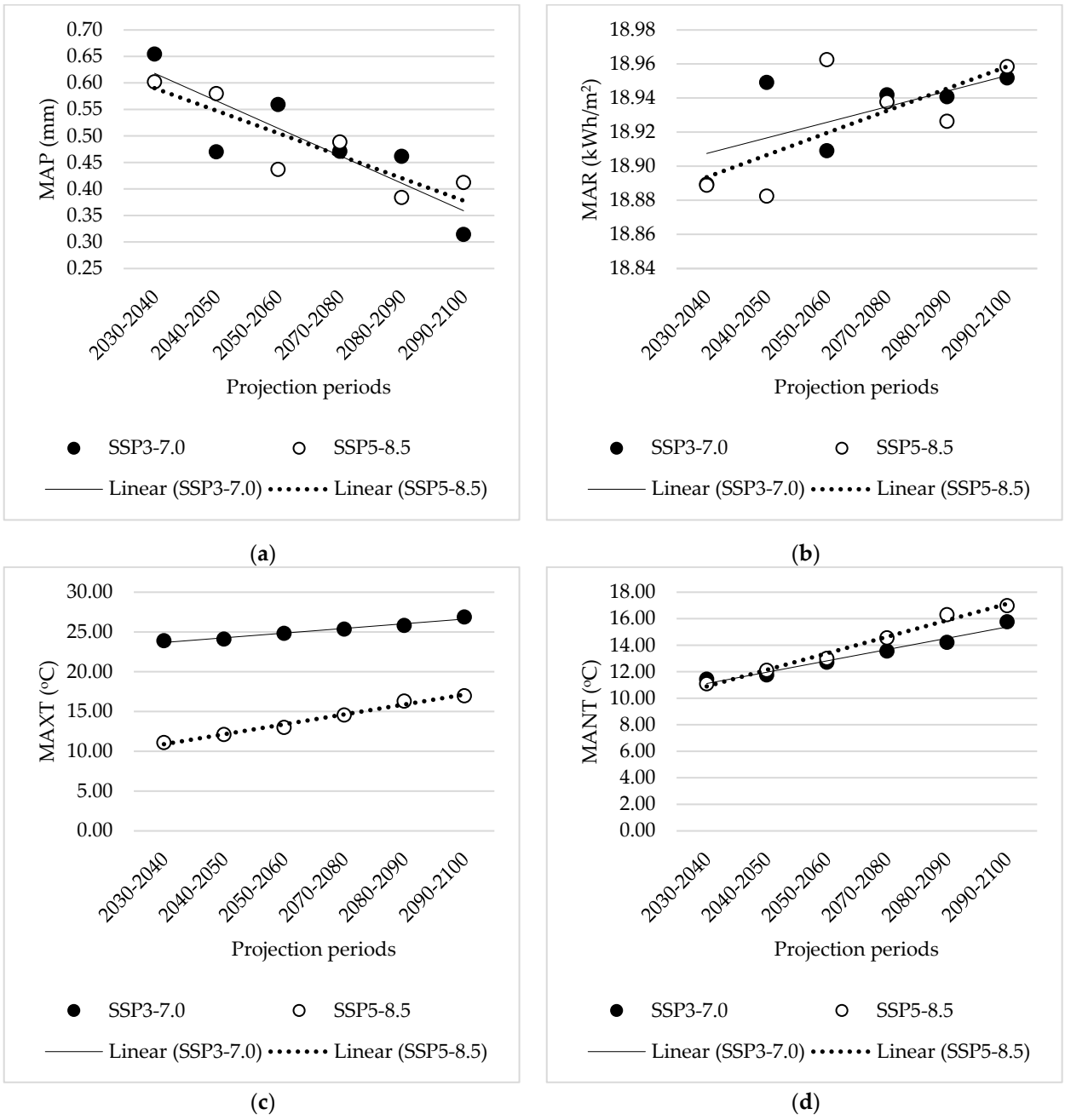


Figure 3. Average ten-year projections of (**a**) MAP (mm), (**b**) MAR (kWh/m^2), (**c**) MAXT (°C), and (**d**) MANT (°C).

Prior to conducting parametric statistical analyses, the normality of the key continuous variables was evaluated using the Shapiro–Wilk test under both climate scenarios (SSP3-7.0 and SSP5-8.5) (Table 6). The tested variables included the WPY, MAP, MAR, MAXT, and MANT. Under SSP3-7.0, all variables exhibited *p*-values greater than 0.05, indicating no significant deviation from a normal distribution (e.g., WPY: $p = 0.7719$; MAXT: $p = 0.5748$). Similarly, under SSP5-8.5, all variables showed *p*-values above the significance threshold, with the lowest observed for WPY ($p = 0.0875$), which still did not indicate a violation of normality. These results confirm that the distributions of all analyzed variables can be considered approximately normal under both scenarios. Accordingly, the use of random forest modeling, correlation analysis, and XGBoost regression models in this study was statistically appropriate and justified.

Under the SSP3-7.0 scenario, the mean production yield was approximately 1118.6 kg/ha, reflecting moderate productivity. The standard deviation (STDV) of 412.2 kg/ha and a coefficient of variation of 36.9% suggest noticeable variability in yield outcomes across the periods or models analyzed. The very low skewness (0.05) indicates that the yield distribution is nearly symmetrical, pointing to a balanced occurrence of both high and low yield years [11]. The minimum yield of 151 kg/ha highlights the potential for significantly poor harvests under more adverse conditions. Regarding climatic conditions, mean annual precipitation is very low at 0.49 mm, typical of arid or semi-arid environments, and exhibits a moderate coefficient of variation (CV = 38.3%). The skewness of 0.70 shows that most years experience below-average rainfall, with occasional spikes. In contrast, solar radiation is highly stable (mean = 18.93 kWh/m^2, CV = 0.45%) and slightly negatively skewed (−0.23), suggesting a consistent energy input with rare instances of reduced radiation, as mentioned by Anbar and Masoud [15] and Mohamed et al. [16] in their studies in Egypt. Maximum temperatures average 25.14 °C with low variation, and the distribution is nearly normal (skewness = 0.13), while minimum temperatures are lower (13.22 °C) and exhibit more variability (CV = 12.3%) with a slightly positive skew, indicating frequent cooler conditions with fewer warmer extremes similar with those conditions reported by Jia et al. [11] in China.

In comparison, the SSP5-8.5 scenario reflects a slightly reduced mean production yield (1048.4 kg/ha) but with increased variability, as evident from a higher STDV (446.4 kg/ha). Unlike SSP3-7.0, the skewness here is negative (−0.51), suggesting that the distribution is left-skewed—in other words, low yields are more common, and extreme yield failures (including cases of zero yield) are possible, as indicated by the minimum value of 0.0 kg/ha. This implies a more vulnerable agricultural outcome under SSP5-8.5, potentially due to harsher climatic stressors [8,18]. Precipitation under SSP5-8.5 is similar in mean (0.49 mm) and variability, though slightly more skewed (0.57), still indicating occasional wet years in a predominantly dry environment. Radiation remains stable (mean = 18.93 kWh/m^2, CV = 0.42%), similar to SSP3-7.0, but with a minor increase in variability. However, temperatures show a clear warming trend: maximum temperature rises to 25.90 °C and minimum temperature to 13.98 °C—both higher than in SSP3-7.0. Their respective STDVs are also greater, indicating a broader range of temperature fluctuations [5]. The skewness values for temperature parameters remain low, suggesting relatively symmetric distributions, though with slightly increased probability of hotter and colder extremes as reported by Anbar and Masoud [15] and Mohamed et al. [16]. These findings aligned with climate anomaly analysis, which was conducted by Al-Shibli et al. [42] over 80 years in Irbid, showing the difference of maximum temperature (−0.5 to 1.5° C) and the highest precipitation variation of 4.25 to −2.04 mm/day in 1974 compared to 2014. It highlighted the soil heat loss during the year except in October, influenced by net radiation, high evaporation and albedo, and warming dry land surface.

3.2.2. Climate Feature Importance for Wheat Yield Across SSP Scenarios

The analysis of feature importance using random forest modeling offers valuable insight into which climate parameters most influence wheat yield across different future climate scenarios [39]. Figure 4 summarizes the importance of each variable across the four evaluated SSP scenarios and periods.

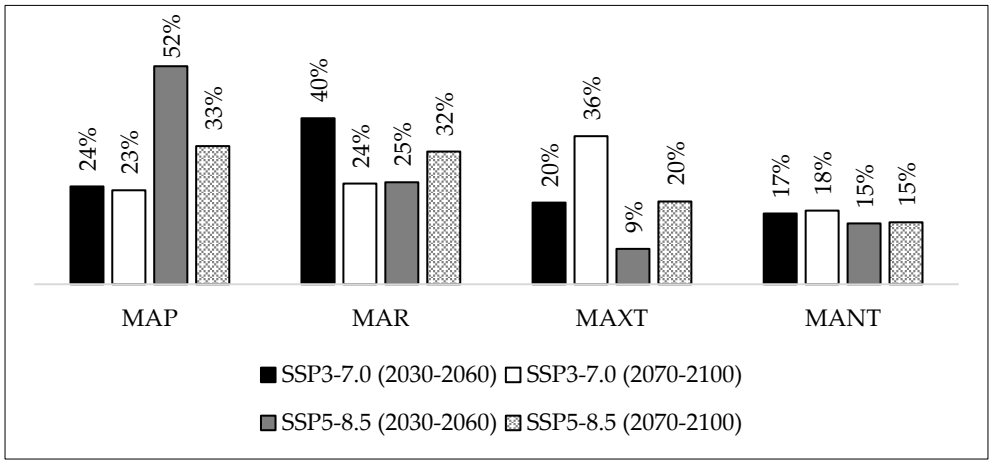


Figure 4. Feature importance for wheat yield across SSP scenarios.

Across all scenarios, precipitation, radiation, and temperature parameters each play variable roles in determining wheat yield, depending on the emissions pathway and future time period [5]. Notably, radiation emerges as the most significant factor in the SSP3-7.0 (2030–2060) scenario, likely due to solar intensity impacts on evapotranspiration, as mentioned by Rezaei et al. [43]. In the SSP3-7.0 (2070–2100) scenario, however, maximum temperature becomes the dominant factor, indicating the increased stress from rising heat levels. Under SSP5-8.5, the pattern shifts significantly. In the 2030–2060 period, precipitation overwhelmingly dominates as the most influential variable (52%), reflecting the importance of water availability during the early intensification of fossil-fueled development [43]. By 2070–2100, feature importance balances out between precipitation and radiation, with a slight decrease in the importance of temperature variables. These results suggest that wheat production under SSP5-8.5 will become increasingly dependent on effective water management, as mentioned by Zhang et al. [44]. However, SSP3-7.0 scenarios emphasize adaptation to temperature extremes [45].

3.2.3. Climate Parameters Correlates with Wheat Production Yield in SSP Scenarios

Correlation analysis was performed to better understand how each climate parameter independently relates to wheat yield [46]. Figure 5 presents the Pearson correlation coefficients between each variable and yield in each scenario.

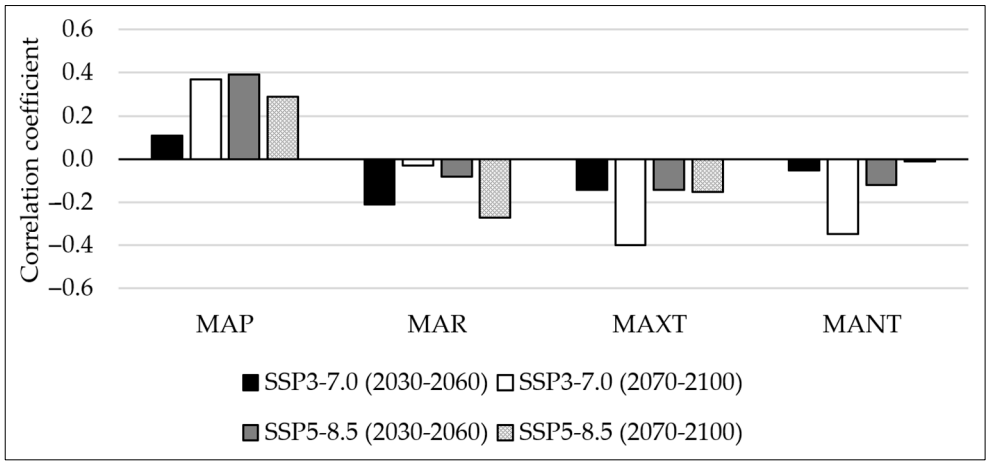


Figure 5. Pearson correlation coefficients between each variable and yield in each scenario.

The correlation values reveal several trends. Precipitation maintains a positive correlation with yield in all cases, with the highest correlation observed in SSP5-8.5 (2030–2060)

and SSP3-7.0 (2070–2100). This indicates the increasing dependency of wheat on adequate rainfall under warming conditions, as stated by Srivastava et al. [46]. Radiation shows consistently negative correlations, particularly in SSP3-7.0 (2030–2060) and SSP5-8.5 (2070–2100), reflecting the potential for yield decline under increased solar stress. Temperature, especially maximum temperature, is more strongly negatively correlated in SSP3-7.0 (2070–2100) than in other scenarios, showing that prolonged exposure to high temperatures could critically reduce wheat yields. Minimum temperature appears to have less direct influence, as shown by weaker correlation values, though its role may be more important in interaction with other factors. These findings underscore the need to tailor climate adaptation strategies to the predominant climatic challenges in each scenario [12,47].

3.3. Model Performance Evaluation

The performance of the XGBoost regression models in predicting wheat yield was evaluated using the coefficient of determination (R^2), which quantifies the proportion of yield variance explained by the selected climate variables [48,49]. Figure 6 represents the average ten-year projected wheat yield production. Table 7 presents the R^2 values alongside the corresponding yield prediction equations for each climate scenario and period.

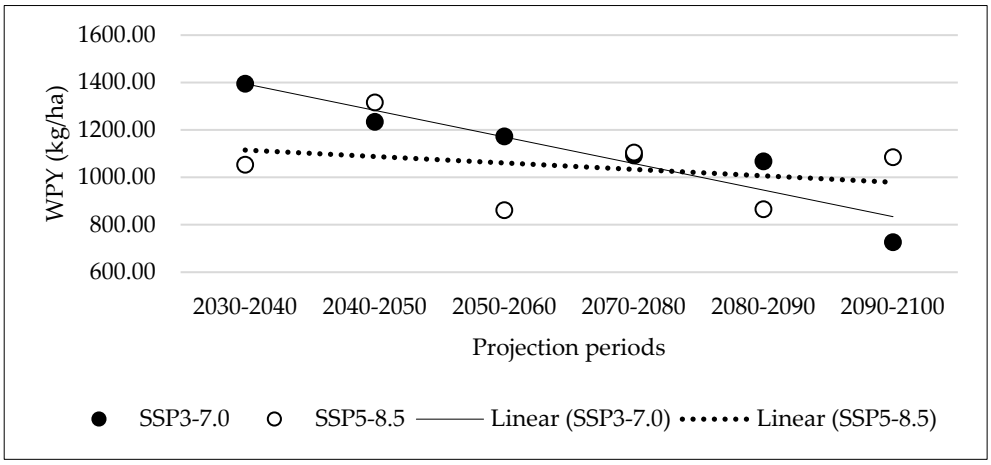


Figure 6. The average ten-year projected wheat yield production.

Table 7. Performance of XGBoost regression models for yield prediction.

SSPs	Years	R^2 Score	Yield Equations Obtained by XGBoost
SSP3-7.0	2030–2060	0.65	$WPY = 30.0 \times MANT + 36.0 \times MAR + 27.0 \times MAP + 14.0 \times MAXT$
	2070–2100	0.73	$WPY = 29.0 \times MAXT + 16.0 \times MANT + 30.0 \times MAR + 33.0 \times MAP$
SSP5-8.5	2030–2060	0.81	$WPY = 64.0 \times MAP + 18.0 \times MANT + 31.0 \times MAR + 19.0 \times MAXT$
	2070–2100	0.74	$WPY = 51.0 \times MAP + 37.0 \times MAR + 17.0 \times MAXT + 21.0 \times MANT$

Among the evaluated scenarios, the SSP5-8.5 projection for 2030–2060 achieved the highest model accuracy, with an R^2 score of 0.81, indicating that climate variables during this period—particularly precipitation—exert a strong and consistent influence on wheat productivity. This finding aligns with previous research emphasizing the dominant role of water availability in yield determination under extreme emission pathways [40]. The predictive equation for this scenario notably highlighted precipitation as the most influential variable, which is consistent with the feature importance results obtained through the random forest model.

In contrast, the SSP3-7.0 scenario for 2030–2060 produced the lowest R^2 score (0.65), suggesting that climate–yield relationships under this scenario are less straightforward,

likely due to regional climate variability and interacting stressors. Interestingly, under SSP3-7.0 for 2070–2100, model performance improved (R^2 = 0.73), with maximum temperature emerging as the dominant limiting factor, reflecting the intensifying impact of prolonged heat stress over time, as highlighted by Yadav et al. [50] and Becker et al. [51].

Meanwhile, the model maintained strong performance under the SSP5-8.5 scenario for 2070–2100, with an R^2 score of 0.74, indicating that even under severe warming, the model effectively captured the combined influences of radiation, precipitation, and thermal stress [52,53].

The current study elaborated two algorithms serving error minimization by two different implementation runs. The bagging algorithm of random forest merges forecasts of established trees independently in contrast to the boosting algorithm that refines errors successively from earlier trees but after tuning data. The two models perform significantly in prediction and provide well-interpretable results [54–56].

These results suggest that predictive accuracy improves when yield is primarily driven by water-related parameters, whereas scenarios influenced by temperature extremes or mixed stressors present greater modeling complexity [7,32,40]. This underscores the importance of developing dynamic, scenario-specific adaptation strategies that consider the dominant climatic drivers in each context [37,44]. Furthermore, the integration of DSSAT simulations with advanced machine learning techniques like XGBoost demonstrates the potential of AI-enhanced analytics in supporting data-driven agricultural decision making and climate-resilient planning, particularly in vulnerable semi-arid regions.

Based on the modeled sensitivity of wheat yield to heat and precipitation extremes, several agronomic adaptation strategies can be considered to improve crop resilience in northern Jordan. These include adjusting planting dates to avoid peak heat during flowering and grain-filling stages and adopting drought- and heat-tolerant wheat varieties already promoted by national breeding programs. Additionally, optimized irrigation scheduling during critical phenological stages could help reduce yield losses under dry spells. Emerging approaches such as nanoparticle-assisted and physiological priming also show promise. For instance, Nagdalian et al. [57] demonstrated that low concentrations of CuO nanoparticles (0.1 mg/L) stabilized with hyaluronic-acid-enhanced wheat seed germination and early seedling vigor, which may improve resilience to early-season stress. Meanwhile, Liu et al. [58] highlighted that high-solid priming applied during booting significantly improved post-anthesis heat stress adaptation in wheat, with potential for transgenerational stress memory, though commercial deployment still requires feasibility assessments. Together, these strategies—ranging from well-established agronomic practices to innovative seed treatments—can offer scalable and climate-informed adaptation options for wheat production under future climatic uncertainty.

Given the emerging evidence on the role of physiological and biochemical priming in improving crop performance under heat and drought stress [57,58], future modeling efforts could benefit from incorporating such mechanisms. This may be achieved by coupling DSSAT with physiological response modules, or by using experimental data to calibrate crop coefficients that reflect primed responses. Integrating these factors could improve the realism and predictive capacity of crop models under complex, stress-prone future scenarios.

3.4. Relevance to Sustainable Development Goals

The findings of this study contribute to advancing the objectives of the United Nations Sustainable Development Goals, particularly SDG 2 (Zero Hunger) and SDG 13 (Climate Action), and align with Atukunda et al. [59]. By simulating the response of wheat yields to projected climate scenarios, this study provides evidence to support sustainable agri-

cultural planning in water-scarce regions. The model-based insights into yield variability under different emission pathways can inform national strategies aimed at enhancing food security and agro-climatic resilience. Furthermore, the identification of climate drivers and critical phenological sensitivities supports the design of climate adaptation measures, contributing to efforts in building resilience to climate-induced yield shocks. These contributions align with global priorities for promoting sustainable food production systems and for integrating climate risk considerations into agricultural policy and planning [60,61].

3.5. Limitations of the Study

While this study provides valuable insights into the projected impacts of climate change on wheat production in northern Jordan, several limitations should be acknowledged:

- The DSSAT model was calibrated using only one wheat variety due to data constraints, limiting applicability across genotypes. Future research should include multiple cultivars to improve representativeness under varying climatic responses.
- Predictor correlation analysis was not conducted due to the dataset's small size and algorithmic nonlinearity. Future studies should apply multicollinearity diagnostics to strengthen machine learning insights.
- The SSP2-4.5, a moderate-emission scenario representing a "middle-of-the-road" socioeconomic pathway with stabilized radiative forcing at 4.5 W/m^2 by 2100, was initially analyzed but excluded due to weak climate–yield associations. While this prevented overinterpretation, it limits representation of moderate climate futures. Extended datasets may better reveal SSP2-4.5 impacts.
- Although global sensitivity analysis methods, such as the Morris or Sobol techniques, were not applied in this study due to computational and scope constraints, their use is recognized as valuable for identifying influential model parameters. Instead, the relative influence of key climatic variables on wheat yield was assessed using machine learning algorithms (random forest and XGBoost), which allowed non-linear relationships and variable importance to be explored. Future integration of global sensitivity methods would enhance understanding of crop model behavior.
- The use of random forest and XGBoost allowed nonlinear climate–yield relationships to be captured effectively through ensemble learning. Future studies may benefit from integrating advanced methods-based interpretability to enhance the transparency and explanatory power of machine learning predictions, particularly in multi-variable climate impact assessments.

4. Conclusions

This study evaluated the projected impacts of shifting precipitation patterns and rising temperatures on wheat productivity in Irbid, Jordan, under two future climate scenarios: SSP3-7.0 and SSP5-8.5. By integrating the DSSAT crop simulation model with machine learning algorithms, the analysis provides critical insights into climate-induced risks and potential adaptation pathways in a semi-arid, climate-sensitive environment.

The calibrated DSSAT-CERES-Wheat model demonstrated strong performance in simulating phenological development, biomass accumulation, and nitrogen uptake across growth stages. It accurately reproduced leaf development and biochemical nitrogen dynamics, particularly during grain filling, with minimal abiotic stress observed. Simulated grain yield and harvest index closely aligned with field measurements, validating the model's reliability in representing both dry matter allocation and nutrient remobilization. Despite minor discrepancies in grain number and unit weight, the model maintained biological realism in overall productivity, supporting its robustness for climate impact assessments.

Under SSP5-8.5 for the near term (2030–2060), water availability—driven by changes in precipitation—was found to be the dominant factor affecting wheat yield, underscoring the need for efficient irrigation and water management. In contrast, maximum temperature emerged as the primary stressor in the long term (2070–2100) under SSP3-7.0, highlighting the escalating threat of heat stress.

In light of the projected impacts of climate change on wheat yield in northern Jordan, several practical adaptation strategies are recommended to enhance resilience in wheat-based production systems. These include shifting planting dates earlier to avoid peak heat stress during flowering and grain filling; adopting drought- and heat-tolerant wheat cultivars that perform better under anticipated conditions; and optimizing irrigation schedules, especially during reproductive stages, to mitigate the effects of rising temperatures and declining rainfall. Additionally, improving irrigation infrastructure and on-farm efficiency will be essential to stabilize yields under rainfall variability. Empowering farmers through seasonal forecasting tools and flexible crop calendars can further support responsive decision making at the farm level [62].

At the policy level, it is essential to promote integrated climate-resilient agricultural frameworks, incorporating early warning systems, farmer training programs, and incentives for adopting climate-smart technologies. These institutional measures should be complemented by continued investment in advanced modeling tools such as DSSAT, especially when coupled with machine learning and data analytics, to enhance scenario planning and risk assessment. Such combined efforts will play a crucial role in strengthening adaptive capacity and promoting sustainable wheat production in Jordan and other climate-vulnerable regions [63].

Author Contributions: Conceptualization, S.E.E.-M. and A.A.S.; methodology, S.E.E.-M. and A.A.S.; software, M.M.Z., S.A.-O. and H.F.A.-J.; validation, M.M.Z., S.A.-O., Q.Y.A.-A. and H.F.A.-J.; formal analysis, S.E.E.-M., M.M.Z. and S.A.-O.; investigation, S.E.E.-M., M.M.Z. and S.A.-O.; resources, M.M.Z., R.T. and Q.Y.A.-A.; data curation, M.M.Z., S.A.-O., Q.Y.A.-A. and F.M.A.-S.; writing—original draft preparation, S.E.E.-M., M.M.Z., S.A.-O. and Q.Y.A.-A.; writing—review and editing, F.M.A.-S., R.T., N.O., S.H.A. and A.M.A.; visualization, Y.A.A., T.M.F.A.-N. and N.O.; supervision, A.A.S.; project administration, A.A.S. All authors have read and agreed to the published version of the manuscript.

Funding: This research received no external funding.

Data Availability Statement: Data are unavailable due to privacy.

Acknowledgments: During the preparation of this manuscript, the authors used ChatGPT-4.5 for the purposes of data handling and grammar corrections. The authors have reviewed and edited the output and take full responsibility for the content of this publication.

Conflicts of Interest: Author Saif Al-Omari was employed by the company Scientific Sustainable Vision Company, Amman 11194, Jordan. The remaining authors declare that the research was conducted in the absence of any commercial or financial relationships that could be construed as a potential conflict of interest. All authors have read and agreed to the published version of the manuscript.

Abbreviations

The following abbreviations are used in this manuscript:

#/g	Number per unit canopy weight grams
%	Percent
°C	Degrees Celsius
°C.d	Degrees Celsius times day
CO_2	Carbon dioxide
CV	Coefficient of variation
DSSAT	The Decision Support System for Agrotechnology Transfer
ESGF	Earth System Grid Federation
g dwt	Grams dewater
GCM	Global Climate Model
kg/ha	Kilogram per hectare
km	Kilometers
kWh/m^2	Kilowatt-hours per square meter
m	Meters
MANT	Mean annual minimum temp
MAP	Mean annual precipitation
MAR	Mean annual radiation
MAXT	Mean annual maximum temp
mg	Milligrams
mm	Millimeters
MOA	Ministry Of Agriculture
MPI-ESM1-2-HR	Meteorology Earth System High-Resolution Model
MWI	Ministry of Water and Irrigation
N	Number of samples
NARC	National Agricultural Research Center
NOAA	National Oceanic and Atmospheric Administration
NRMSE	Normalized root mean square error
O_i	Observed yield
PBC	Public Benefit Corporation
pH	Potential of hydrogen
P_i	Predicted yield
QMM	Quantile Mapping Method
RStudio	R Programming Language Studio
R^2 score	Coefficient of determination
RMSE	Root mean square error
SOC	Soil organic carbon
SSP	Shared socioeconomic pathways
WPY	Wheat production yield
XGBoost	EXtreme Gradient Boosting
$\overline{y}$	Mean value of the predicted and of observed yield

References

1. Abu-Afifeh, Q.; Rahbeh, M.; Al-Afeshat, A.; Al-Omari, S.; Qutishat, T.A.; Brezat, A.; Alkayed, A. Dam Sustainability's Interdependency with Climate Change and Dam Failure Drivers. *Sustainability* **2023**, *15*, 16239. [CrossRef]
2. Al-Afeshat, A.; Zoubi, M.M.; Abu Afifeh, Q.Y.; Al-Jawaldeh, H.; Qutishat, T.A.; Masoud, A.M.N.; Rahbeh, M. Interrelation of Dams Sustainability with the Local Communities and Water Quality. *Global J. Environ. Sci. Manag.* **2025**, *11*, 157–176.
3. Obeidat, N.; Abu Awwad, A.; Al-Salaymeh, A.; Bresciani, R.; Masi, F.; Rizzo, A.; AlBtoosh, J.; Zoubi, M.M. Ground-Based Green Façade for Enhanced Greywater Treatment and Sustainable Water Management. *Water* **2025**, *10*, 346. [CrossRef]
4. Farooq, A.; Farooq, N.; Akbar, H.; Hassan, Z.U.; Gheewala, S.H. A Critical Review of Climate Change Impact at a Global Scale on Cereal Crop Production. *Agronomy* **2023**, *13*, 162. [CrossRef]

5. Hroub, H.A.; Rahbeh, M.; Zoubi, M.M.; Abu-Afifeh, Q.Y.; Al-Jawaldeh, H.; Obeidat, N. Projection of Future Temperature Variations in River Basins under Climate Change Scenarios Using General Circulation Models. *Global J. Environ. Sci. Manag.* **2025**, *11*, 403–426.
6. Al-Addous, M.; Bdour, M.; Alnaief, M.; Rabaiah, S.; Schweimanns, N. Water Resources in Jordan: A Review of Current Challenges and Future Opportunities. *Water* **2023**, *15*, 3729. [CrossRef]
7. Corbeels, M.; Chirat, G.; Messad, S.; Thierfelder, C. Performance and Sensitivity of the DSSAT Crop Growth Model in Simulating Maize Yield under Conservation Agriculture. *Eur. J. Agron.* **2016**, *76*, 41–53. [CrossRef]
8. Al-Bakri, J.; Suleiman, A.; Abdulla, F.; Ayad, J. Potential Impact of Climate Change on Rainfed Agriculture of a Semi-Arid Basin in Jordan. *Phys. Chem. Earth* **2011**, *36*, 125–134. [CrossRef]
9. Waffa, R.; Benoit, G. Simulation of Climate Change Impact on Wheat Production in the Tiaret Region of Algeria Using the DSSAT Model. *Eur. Sci. J.* **2015**, *11*, 249–259.
10. Dawoud, R.A.; Noreldin, T.; Shehata, R.S.; Moawod, H.; Kasem, A. Calibration of the DSSAT-CERES Wheat Crop Model under Scenarios of Climate Change Adaptation and Biotic Stress. *J. Adv. Biol. Biotechnol.* **2023**, *26*, 52–64. [CrossRef]
11. Jia, D.; Wang, C.; Han, Y.; Huang, H.; Xiao, H. Impact of Climate Change on the Yield and Water Footprint of Winter Wheat in the Haihe River Basin, China. *Atmosphere* **2022**, *13*, 630. [CrossRef]
12. Althalaj, T.D.A.; Al-Shibli, F.M.; Alassaf, A.A. Assessment of Rainfed Wheat Productivity in a Changing Climate in Irbid, Jordan Using Statistical Downscaling and Random Forest Regression Prediction under RCP4.5 & 8.5 Pathways. *Environ. Sustain. Indic.* **2025**, *25*, 100545.
13. Al-Shdeifat, M. The Impact of Climate Change on Wheat Based on Multiple Climate Scenarios: A Case Study in Irbid Governorate. Master's Thesis, Jerash University, Jerash, Jordan, 2022; pp. 1–96.
14. Al-Titi, M. Impact of Rainfall and Temperature Change on Field Crops Production in Karak Governorate—Jordan. Master's Thesis, Jerash University, Jerash, Jordan, 2020; pp. 1–73.
15. Anbar, M.; Masoud, S. The Impact of Climate Change on Certain Agricultural Crops in Fayoum Governorate, Egypt. *Cent. Geogr. Cartogr. Res. J.* **2021**, *18*, 625–704.
16. Mohamed, H.S.; Sherif, S.; El-Saify, E.; Shehab, S.M. Measuring the Impact of Changing Climatic Factors on Wheat Crop in Egypt. *J. Adv. Agric. Res.* **2018**, *23*, 256–269.
17. Halawa, B. Evaluating the Impact of Climate Change on Maize Productivity Using the AquaCrop Model in Mokhtariya Research Station, Homs, Syria. Master's Thesis, Homs University, Homs, Syria, 2022; pp. 1–100.
18. Al-Zraiqat, J. The Impact of Agriculture on Climate Change. *Arab J. Sci. Publ.* **2022**, *A*, 378–388.
19. Obeidat, N.; Abu-Awwad, A.; Al-Salaymeh, A.S.; AlBtoosh, J.; Zoubi, M.M.; Abu-Afifeh, Q.Y.; Seif, M.A.; Hroub, H.; Arabiat, O. Social Acceptance of Water Quality through Decentralized Greywater Treatment Using Green Wall System. *Global J. Environ. Sci. Manag.* **2025**, *11*, 519–532.
20. Mehrabi, F.; Sepaskhah, A.R. Winter Wheat Yield and DSSAT Model Evaluation in a Diverse Semi-Arid Climate and Agronomic Practices. *Int. J. Plant Prod.* **2019**, *14*, 221–243. [CrossRef]
21. Müller, W.A.; Jungclaus, J.H.; Mauritsen, T.; Baehr, J.; Bittner, M.; Budich, R.; Bunzel, F.; Esch, M.; Ghosh, R.; Haak, H.; et al. A Higher-Resolution Version of the Max Planck Institute Earth System Model (MPI-ESM1.2-HR). *J. Adv. Model. Earth Syst.* **2018**, *10*, 1383–1413. [CrossRef]
22. Mauritsen, T.; Bader, J.; Becker, T.; Behrens, J.; Bittner, M.; Brokopf, R.; Brovkin, V.; Claussen, M.; Crueger, T.; Esch, M.; et al. Developments in the MPI-M Earth System Model Version 1.2 (MPI-ESM1.2) and Its Response to Increasing CO_2. *J. Adv. Model. Earth Syst.* **2019**, *11*, 998–1038. [CrossRef]
23. Meinshausen, M.; Nicholls, Z.R.J.; Lewis, J.; Gidden, M.J.; Vogel, E.; Freund, M.; Beyerle, U.; Gessner, C.; Nauels, A.; Bauer, N.; et al. The Shared Socio-Economic Pathway (SSP) Greenhouse Gas Concentrations and Their Extensions to 2500. *Geosci. Model Dev.* **2020**, *13*, 3571–3605. [CrossRef]
24. Sørland, S.L.; Brogli, R.; Pothapakula, P.K.; Russo, E.; Van de Walle, J.; Ahrens, B.; Anders, I.; Bucchignani, E.; Davin, E.L.; Demory, M.-E.; et al. COSMO-CLM Regional Climate Simulations in the Coordinated Regional Climate Downscaling Experiment (CORDEX) Framework: A Review. *Geosci. Model Dev.* **2021**, *14*, 5125–5154. [CrossRef]
25. Gutiérrez, J.M.; Maraun, D.; Widmann, M.; Huth, R.; Hertig, E.; Benestad, R.; Roessler, O.; Wibig, J.; Wilcke, R.; Kotlarski, S.; et al. An Intercomparison of a Large Ensemble of Statistical Downscaling Methods over Europe: Results from the VALUE Perfect Predictor Cross-Validation Experiment. *Int. J. Climatol.* **2018**, *39*, 3750–3785. [CrossRef]
26. Tita, D. Pathways for the Sustainable Intensification of Wheat Production under Current and Future Climate Change Scenarios in the Mediterranean Region. Master Thesis, Soil Physics and Land Management Group, Wageningen University, Wageningen, The Netherlands, 2024; pp. 1–36.
27. Banerjee, K.; Dutta, S.; Das, S.; Sadhukhan, R. Crop Simulation Models as Decision Tools to Enhance Agricultural System Productivity and Sustainability—A Critical Review. *Technol. Agron.* **2025**, *5*, e002. [CrossRef]

28. Chapagain, R.; Huth, N.; Remenyi, T.A.; Mohammed, C.L.; Ojeda, J.J. Assessing the Effect of Using Different APSIM Model Configurations on Model Outputs. *Ecol. Modell.* **2023**, *483*, 110451. [CrossRef]
29. Demestihas, C.; Plénet, D.; Génard, M.; Garcia de Cortazar-Atauri, I.; Launay, M.; Ripoche, D.; Beaudoin, N.; Simon, S.; Charreyron, M.; Raynal, C.; et al. Analyzing Ecosystem Services in Apple Orchards Using the STICS Model. *Eur. J. Agron.* **2018**, *94*, 108–119. [CrossRef]
30. Carozzi, M.; Martin, R.; Klumpp, K.; Massad, R.S. Effects of Climate Change in European Croplands and Grasslands: Productivity, Greenhouse Gas Balance and Soil Carbon Storage. *Biogeosciences* **2022**, *19*, 3021–3050. [CrossRef]
31. Bregaglio, S.; Ginaldi, F.; Raparelli, E.; Fila, G.; Bajocco, S. Improving Crop Yield Prediction Accuracy by Embedding Phenological Heterogeneity into Model Parameter Sets. *Agric. Syst.* **2023**, *209*, 103666. [CrossRef]
32. Gobezie, A.; Ademe, D.; Sharma, L.K. CERES-Maize (DSSAT) Model Applications for Maize Nutrient Management across Agroecological Zones: A Systematic Review. *Plants* **2025**, *14*, 661. [CrossRef]
33. El Sabagh, A.; Islam, M.S.; Skalicky, M.; Ali Raza, M.; Singh, K.; Anwar Hossain, M.; Hossain, A.; Mahboob, W.; Iqbal, M.A.; Ratnasekera, D.; et al. Salinity Stress in Wheat (*Triticum Aestivum* L.) in the Changing Climate: Adaptation and Management Strategies. *Front. Agron.* **2021**, *3*, 661932. [CrossRef]
34. Tahir, M.; Arshad, M.A.; Akbar, B.A.; Bibi, A.; Ain, Q.U.; Bilal, A.; Arqam, S.M.; Asif, M.; Ishtiaq, M.H.; Rasheed, H.U.; et al. Integrated Nitrogen and Irrigation Management Strategies for Sustainable Wheat Production: Enhancing Yield and Environmental Efficiency. *J. Pharmacogn. Phytochem.* **2024**, *13*, 209–222. [CrossRef]
35. Mentaschi, L.; Besio, G.; Cassola, F.; Mazzino, A. Problems in RMSE-Based Wave Model Validations. *Ocean Modell.* **2013**, *72*, 53–58. [CrossRef]
36. Batool, D.; Shahbaz, M.; Shahzad Asif, H.; Shaukat, K.; Alam, T.M.; Hameed, I.A.; Ramzan, Z.; Waheed, A.; Aljuaid, H.; Luo, S. A Hybrid Approach to Tea Crop Yield Prediction Using Simulation Models and Machine Learning. *Plants* **2022**, *11*, 1925. [CrossRef]
37. Arshad, M.N.; Ahmad, A.; Wajid, S.A.; Cheema, M.J.M.; Schwartz, M.W. Adapting DSSAT Model for Simulation of Cotton Yield for Nitrogen Levels and Planting Dates. *Agron. J.* **2017**, *109*, 2639–2648. [CrossRef]
38. Pant, J.; Pant, R.P.; Kumar Singh, M.; Pratap Singh, D.; Pant, H. Analysis of Agricultural Crop Yield Prediction Using Statistical Techniques of Machine Learning. *Mater. Today Proc.* **2021**, *46*, 10922–10926. [CrossRef]
39. Breiman, L. Random Forests. *Mach. Learn.* **2001**, *45*, 5–32. [CrossRef]
40. Ravi, R.; Baranidharan, B. Crop Yield Prediction Using XG Boost Algorithm. *Int. J. Recent Technol. Eng.* **2020**, *8*, 3516–3520. [CrossRef]
41. Nielsen, D. Tree Boosting with XGBoost-Why Does Xgboost Win "Every" Machine Learning Competition? Master's Thesis, NTNU: Norwegian University of Science and Technology, Trondheim, Norway, 2016.
42. Al-Shibli, F.; Maher, W.; Ottom, M.A.; Al-Bakri, J.T. Estimating Soil Heat Flux in Jordan Based on ERA5 Parameters and NCEP/NCAR Energy Outputs: Definite Radiative Forcing of Climate Change Using PCA. *Earth Syst. Environ.* **2024**, *8*, 369–393. [CrossRef]
43. Rezaei, A.; Karami, K.; Tilmes, S.; Moore, J.C. Future Water Storage Changes over the Mediterranean, Middle East, and North Africa in Response to Global Warming and Stratospheric Aerosol Intervention: Earth System Dynamics. *Earth Syst. Dyn.* **2024**, *15*, 91–108. [CrossRef]
44. Zhang, C.; Chen, J.; Hu, K.; He, Y. Enhancing Wheat Protein through Low-Water-Fertility under Climate Change without Yield Penalty. *Agric. Water Manag.* **2024**, *300*, 108909. [CrossRef]
45. Deepa, R.; Kumar, V.; Sundaram, S. A Systematic Review of Regional and Global Climate Extremes in CMIP6 Models under Shared Socio-Economic Pathways. *Theor. Appl. Climatol.* **2024**, *155*, 2523–2543. [CrossRef]
46. Srivastava, A.K.; Safaei, N.; Khaki, S.; Lopez, G.; Zeng, W.; Ewert, F.; Gaiser, T.; Rahimi, J. Winter Wheat Yield Prediction Using Convolutional Neural Networks from Environmental and Phenological Data. *Sci. Rep.* **2022**, *12*, 3215. [CrossRef] [PubMed]
47. Abbass, K.; Qasim, M.Z.; Song, H.; Murshed, M.; Mahmood, H.; Younis, I. A Review of the Global Climate Change Impacts, Adaptation, and Sustainable Mitigation Measures. *Environ. Sci. Pollut. Res.* **2022**, *29*, 42539–42559. [CrossRef]
48. Li, Y.; Zeng, H.; Zhang, M.; Wu, B.; Zhao, Y.; Yao, X.; Cheng, T.; Qin, X.; Wu, F. A County-Level Soybean Yield Prediction Framework Coupled with XGBoost and Multidimensional Feature Engineering. *Int. J. Appl. Earth Obs. Geoinf.* **2023**, *118*, 103269. [CrossRef]
49. Li, X.; Li, Z. Global Water Availability and Its Distribution under the Coupled Model Intercomparison Project Phase Six Scenarios. *Int. J. Climatol.* **2022**, *42*, 5748–5767. [CrossRef]
50. Yadav, M.R.; Choudhary, M.; Singh, J.; Lal, M.K.; Jha, P.K.; Udawat, P.; Gupta, N.K.; Rajput, V.D.; Garg, N.K.; Maheshwari, C.; et al. Impacts, Tolerance, Adaptation, and Mitigation of Heat Stress on Wheat under Changing Climates. *Int. J. Mol. Sci.* **2022**, *23*, 2838. [CrossRef]
51. Becker, R.; Schüth, C.; Merz, R.; Khaliq, T.; Usman, M.; Beek, T.a.d.; Kumar, R.; Schulz, S. Increased Heat Stress Reduces Future Yields of Three Major Crops in Pakistan's Punjab Region despite Intensification of Irrigation. *Agric. Water Manag.* **2023**, *281*, 108243. [CrossRef]

52. Farhad, M.; Kumar, U.; Tomar, V.; Bhati, P.K.; Krishnan, J.N.; Kishwar-E-Mustarin, N.; Barek, V.; Brestic, M.; Hossain, A. Heat Stress in Wheat: A Global Challenge to Feed Billions in the Current Era of the Changing Climate. *Front. Sustain. Food Syst.* **2023**, *7*, 247–256. [CrossRef]
53. Lesk, C.; Anderson, W.; Rigden, A.; Coast, O.; Jägermeyr, J.; McDermid, S.; Davis, K.F.; Konar, M. Compound Heat and Moisture Extreme Impacts on Global Crop Yields under Climate Change. *Nat. Rev. Earth Environ.* **2022**, *3*, 872–889. [CrossRef]
54. Januschowski, T.; Wang, Y.; Torkkola, K.; Erkkilä, T.; Hasson, H.; Gasthaus, J. Forecasting with Trees. *Int. J. Forecast.* **2022**, *38*, 1473–1481. [CrossRef]
55. Syam, N.; Kaul, R. Random Forest, Bagging, and Boosting of Decision Trees. *Mach. Learn. Artif. Intell. Mark. Sales* **2021**, *2021*, 139–182.
56. Salman, H.A.; Kalakech, A.; Steiti, A. Random Forest Algorithm Overview. *Babylon. J. Mach. Learn.* **2024**, *2024*, 69–79. [CrossRef] [PubMed]
57. Nagdalian, A.; Blinov, A.; Golik, A.; Gvozdenko, A.; Rzhepakovsky, I.; Avanesyan, S.; Pirogov, M.; Askerova, A.; Shariati, M.A.; Mubarak, M.S. Nano-Priming of Pea (*Pisum Sativum* L.) Seeds with CuO Nanoparticles: Synthesis, Stabilization, Modeling, Characterization, and Comprehensive Effect on Germination and Seedling Parameters. *Food Chem.* **2025**, *478*, 143569. [CrossRef] [PubMed]
58. Liu, H.; Able, A.J.; Able, J.A. Priming Crops for the Future: Rewiring Stress Memory. *Trends Plant Sci.* **2021**, *27*, 699–716. [CrossRef]
59. Atukunda, P.; Eide, W.B.; Kardel, K.R.; Iversen, P.O.; Westerberg, A.C. Unlocking the Potential for Achievement of the UN Sustainable Development Goal 2—"Zero Hunger"—In Africa: Targets, Strategies, Synergies and Challenges. *Food Nutr. Res.* **2021**, *65*, 1–11. [CrossRef]
60. Khanal, U.; Wilson, C.; Rahman, S.; Lee, B.L.; Hoang, V.-N. Smallholder Farmers' Adaptation to Climate Change and Its Potential Contribution to UN's Sustainable Development Goals of Zero Hunger and No Poverty. *J. Cleaner Prod.* **2021**, *281*, 124999. [CrossRef]
61. Filho, W.L.; Wall, T.; Salvia, A.L.; Dinis, M.A.P.; Mifsud, M. The Central Role of Climate Action in Achieving the United Nations' Sustainable Development Goals. *Sci. Rep.* **2023**, *13*, 20582. [CrossRef]
62. Nazari, M.; Mirgol, B.; Salehi, H. Climate Change Impact Assessment and Adaptation Strategies for Rainfed Wheat in Contrasting Climatic Regions of Iran. *Front. Agron.* **2021**, *3*, 806146. [CrossRef]
63. Alsafadi, K.; Bi, S.; Abdo, H.G.; Almohamad, H.; Alatrach, B.; Srivastava, A.K.; Al-Mutiry, M.; Bal, S.K.; Chandran, M.A.S.; Mohammed, S. Modeling the Impacts of Projected Climate Change on Wheat Crop Suitability in Semi-Arid Regions Using the AHP-Based Weighted Climatic Suitability Index and CMIP6. *Geosci. Lett.* **2023**, *10*, 20. [CrossRef]

Disclaimer/Publisher's Note: The statements, opinions and data contained in all publications are solely those of the individual author(s) and contributor(s) and not of MDPI and/or the editor(s). MDPI and/or the editor(s) disclaim responsibility for any injury to people or property resulting from any ideas, methods, instructions or products referred to in the content.